

A Strategy in The Design of Micellar Shape for Cancer Therapy

Tao Chen, Xing Guo, Xian Liu, Shuai Shi, Jie Wang, Chunli Shi, Zhiyong Qian, and Shaobing Zhou*

For cancer therapy, optimization of carrier features is necessary to effectively deliver the targeting agents to tumor sites. Biodegradable poly(ether-anhydrides) micelles with filamentous, rod-like, and spherical shapes are fabricated. Their size and morphology are characterized by AFM and TEM. The encapsulation of doxorubicin hydrochloride (DOX) into the micelles does not impact their shape. The effect of micellar shape on the drug loading capacity and encapsulation efficiency, as well as *in vitro* drug release, is investigated. The cellular uptakes are evaluated using fluorescence microscopy, confocal laser scanning microscopy and flow cytometry on co-cultures of human hepatoblastoma cell line (HepG2), lung epithelial cancer cell line (A549), and human nasopharyngeal epidermoid carcinoma cells (KB) and fibroblast normal cells mixed with the different shapes of DOX-loaded micelles. The results show that the spherical DOX-loaded micelles are more readily taken up by all types of cells. The impact of micellar shape on *in vivo* antitumor function is also assessed from changes of tumor volume, body weight loss, and survival rate of 4T1-bearing mice and the immunostaining of tumor sections for analysis of tumor cell proliferation. The results reveal that the filamentous DOX-loaded micelles possess the highest safety to body and the best therapeutic effects to artificial solid tumors. Therefore, the filamentous shape is deemed the most suitable morphology for design and engineering of drug vehicles for cancer therapy.

design features is necessary to improve targeting efficiency towards tumor tissue. To date, aside from polymer composition, size^[2–7] and surface chemistry^[8–13] are the two important parameters have been most extensively studied. However, previous investigations on the properties of drug carriers have mainly been focused on spherical particles. In last few years some research has reported that difference in shape is also a critical parameter, and even plays a key role in controlling the performance of particles in a controlled release system for drugs.^[14] A suitable geometry is therefore vital to enhancing particle function in biomedical applications, and fabricating optimized drug-delivery vehicles.

Current drug delivery literature is beginning to reflect that particle shape is also a critical parameter in influencing carrier behavior *in vitro* and *in vivo*, and more and more evidence shows that its role is independent of other parameters during the cell-particle interaction. The efficiency of a drug carrier is determined by that interaction. Carrier shape has been shown to have a profound effect on

drug loading capacity,^[15–18] their cellular internalization,^[14,19–21] circulation half life,^[22,23] targeting efficiency^[24,25] and phagocytosis.^[14,20,26] However, the precise role of particle shape in drug delivery has not been fully elucidated due to a bottleneck of easy-to-use methods available to control particle shape. For example, the Mitragotri and Desimone groups reported separately that shape is an essential property of a particle and has an important role in regulating biological responses and related applications in biotechnology.^[27,28] Sometimes particle shape plays a dominant role in response to cell and tissue, and it is well known that spherical particles must be less than 200 nm in diameter to pass through the spleen, but disk-shaped, flexible red blood cells pass unhindered through the spleen despite their large size.

The investigation into the impact of particle shape on drug delivery systems is still in its early stages, and the particle dimension employed is often on the microscale, most likely due for ease of observation. However, in drug delivery systems intended for cancer therapy, it has been documented that nanoscale carriers can improve the tumor drug delivery and therapeutic efficiency,^[29,30] which is mostly ascribed to its the

1. Introduction

Design and engineering of novel carriers for drug delivery have long been issues of active research.^[1] Optimization of the carrier

T. Chen, Dr. X. Guo, Dr. X. Liu, J. Wang, Prof. S. B. Zhou
School of Materials Science and Engineering
Key Laboratory of Advanced Technologies of Materials
Ministry of Education
Southwest Jiaotong University
Chengdu, 610031, P. R. China
E-mail: szhou@seas.harvard.edu; shaobingzhou@hotmail.com

Dr. S. Shi, Prof. Z. Y. Qian
State Key Laboratory of Biotherapy
West China Hospital
West China Medicine School
Sichuan University
Chengdu, 610041, P. R. China
C. L. Shi, Prof. S. B. Zhou
School of Life Science and Engineering
Southwest Jiaotong University
Chengdu 610031, Sichuan, P.R. China

DOI: 10.1002/adhm.201100040



ability to pass through cellular barriers and evade phagocytosis by macrophages during delivery.^[31] Nanoparticles deployed for cancer therapy thus far include polymeric nanoparticles,^[32] liposomes,^[33] polymeric micelles,^[34,35] polymersomes,^[36] and inorganic nanoparticles.^[37] Polymeric micelles, as one of the most important classes of nanocarriers, are self-assembled from amphiphilic polymers with a hydrophobic core and surrounding hydrophilic shell, and achieve desirable efficiency and excellent biocompatibility in drug delivery. They display many merits, such as nanometer size, enhanced solubility of hydrophobic antitumor drugs, relatively high stability due to their low critical micelle concentration (CMC), and prolonged circulation owing to their high water solubility.^[38–40] Various micellar shapes can be obtained by altering polymer structure, concentration, types of solvent, and temperature.^[41]

Herein, biodegradable polymer micelles with diverse shapes were employed to investigate drug release behavior and cellular internalization in tumor cells *in vitro* and their therapeutic effect on solid tumors *in vivo*. It is necessary to study in detail the influence of micellar shape on performance in antitumor drug delivery. Inspiringly, some literature is beginning to be devoted to the importance of micellar shape with the rapid development of polymer micelles for potential applications in nanomedicine.^[16,18,22,42–44] Furthermore, among those micelles with diverse shape, flexible filomicelles are also inclined to aggregate in the tumor site relative to other normal organs due to the enhanced permeation and retention (EPR) effect.^[18,22] Consequently the micellar morphology is worthy of careful consideration in the design and evaluation of drug delivery vehicles.

In the study, amphiphilic poly(ether-anhydrides) terpolymers composed of sebacic acid (SA), 1,3-bis(carboxyphenoxy) propane (CPP), and poly(ethylene glycol) (PEG) were synthesized via melt-condensation polymerization. Combining the advantages of PEG and polyanhydride,^[45–47] biodegradable polymer micelles with spherical (S), filamentous (F) and rod-like (R) shapes were fabricated and evaluated as doxorubicin (DOX) delivery vehicles. The main performance indicators including drug loading, *in vitro* drug release, cytotoxicity, and cellular uptake efficiency of DOX-loaded micelles were investigated. In addition, the effect of the micellar shape on anti-tumor efficacy was investigated in order to evaluate passive targeting in 4T1 tumor models in Balb/c mice.

2. Results and Discussion

2.1. Characterizations of Amphiphilic Terpolymer

To confirm successful synthesis of the poly(ether-anhydride) terpolymer, FT-IR and ¹H NMR spectroscopy were used to confirm the chemical structure. The FT-IR spectra of the PEG2000 and poly(PEG:SA:CPP) terpolymer are represented in Figure 1A. It can be seen that for the terpolymer, a typically strong stretching band at 1728 cm⁻¹ is attributed to the C = O stretching vibrations of the ester carbonyl group, which indicates successful combination between the hydroxyl group of the PEG and the estolide groups of the SA, CPP prepolymer. Also, a C=O stretching vibration appears at 1820 cm⁻¹, which

is ascribed to the characteristic peak of anhydride bonds, indicating combination among the anhydride prepolymers. ¹H-NMR spectroscopy was employed to further certify the formation of poly(PEG:SA:CPP) terpolymers. The ¹H NMR spectrum of poly(PEG:SA:CPP) is illustrated in Figure 1B. The ¹H NMR resonance signals from the methylene protons of PEG appeared at 3.68 ppm. The chemical shifts at 1.33, 1.65 and 2.46 ppm were attributed to the methylene protons of SA and peaks at 1.66, 4.26, 6.96 and 7.98 ppm were ascribed to the methylene protons of CPP. These results are in accord with the information acquired from the FT-IR spectra. The presence of the characteristic chemical shifts also confirmed successful polycondensation among the SA and CPP prepolymers and PEG2000. Furthermore, the actual ratios of PEG, SA, and CPP in the terpolymer were calculated from the integrated area of distinct chemical shifts on ¹H-NMR spectrum. All the synthesized products have approximate ratios of monomer units to the feeding compositions, which are summarized in Table 1.

2.2. Size and Morphology of the Polymeric Micelles

The amphiphilic terpolymer can self-assemble into micelles with diverse shapes in water by altering the ratio of PEG and SA in polymer backbone. The micellar morphology and size were characterized with AFM, TEM and DLS, as shown in Figure 1C–K and Table 1. TEM images of the blank polymeric micelles show that the spherical, rod-like, and filamentous shapes formed corresponding to PEG:SA:CPP molar ratios of 40:40:20, 30:50:20 and 20:60:20, respectively. The average diameter of the micelles is about 60 nm, and the length approaches ca. 1200 nm and 280 nm for filamentous and rod-like micelles, respectively. Figure 1F–K shows the AFM images of the blank and DOX-loaded micelles of the poly(PEG:CPP:SA) terpolymers with different PEG:SA:CPP molar ratios. We found that the micelles also take on spherical, rod-like and filamentous shapes by changing the ratio of PEG and SA, which is in good agreement with the result of the TEM investigation. Moreover, we found that the DOX loading in micelles has almost no effect on their morphology, the only difference being a slight increase in diameter. This can be ascribed to the change of the nature of hydrophilic corona and hydrophobic core after the drug is encapsulated or bound to the micelles.^[43] In addition, from Table 1 we can see that the Z-average values of the micelles obtained from DLS are about 65 nm, 120 nm and 268 nm for S, R and F, respectively. It is worth noting that the Z-average values of diameter were very different from those measured by AFM and TEM directly, especially for R and F. The reason is that the average diameter of nonspherical particles from DLS measurement derives from the correlation function analysis based on the supposition that the micelles are spherical.^[48]

As is well known, the diameter of polymer particles as a drug carrier used in the treatment of cancers should be on the nanoscale, which can extravasate and accumulate in the tumor site passively through the enhanced permeation and retention (EPR) effect (particles smaller than 500 nm).^[29,30] In addition, the rod-like and filamentous micelles have higher aspect ratio, especially for the filamentous micelle, which possess bigger

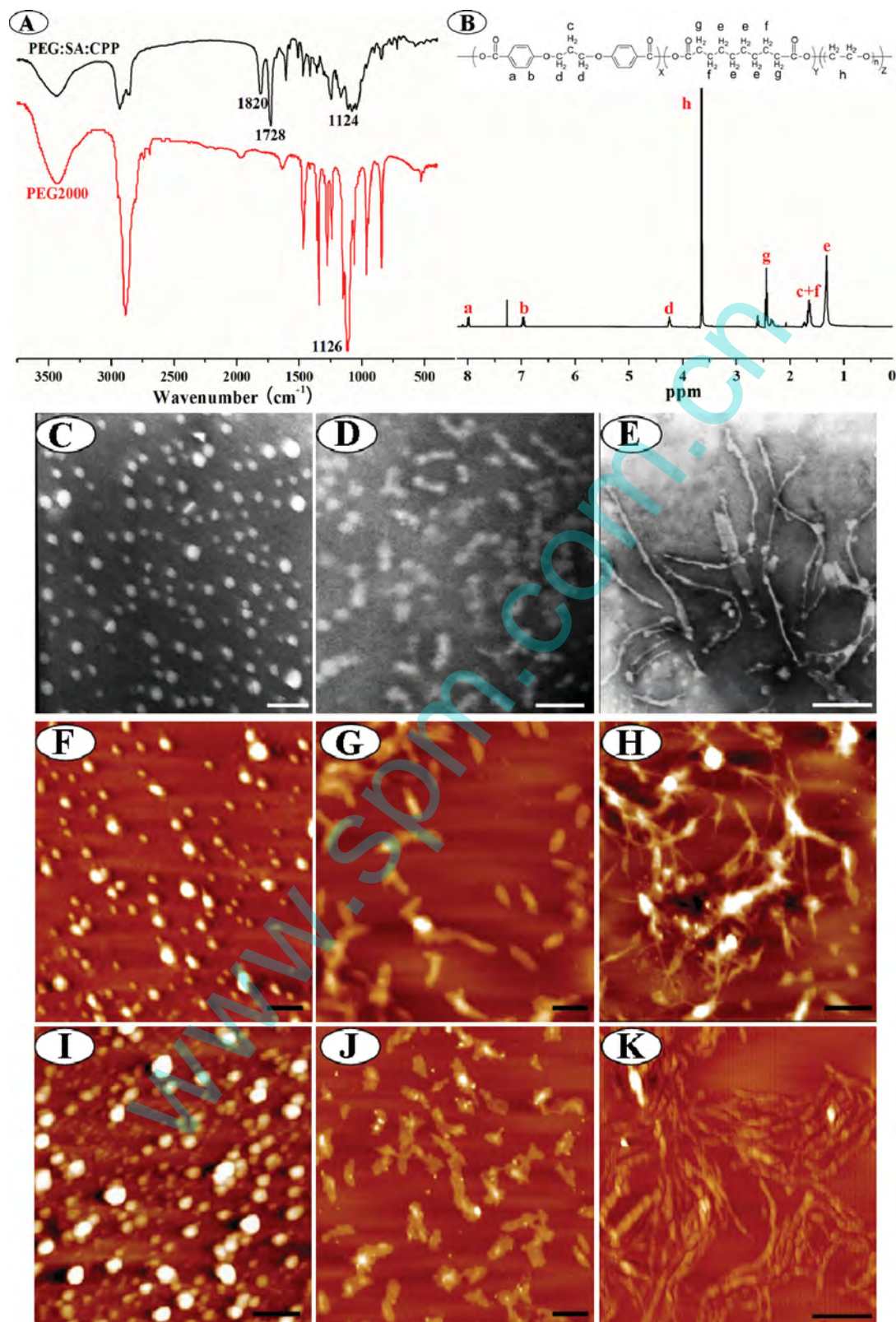


Figure 1. FT-IR spectra of PEG and poly(PEG:SA:CPP) (30:50:20) terpolymer (A); ¹H NMR spectrum of poly(PEG:SA:CPP) (30:50:20) terpolymer (B); TEM images of the blank micelles prepared from poly(PEG:SA:CPP) with PEG/SA/ CPP ratios of 20:60:20 (C), 30:50:20 (D) and 40:40:20 (E); AFM images of the blank micelles and DOX-loaded micelles prepared from poly(PEG:SA:CPP) with PEG/SA/ CPP ratios of 20:60:20 (F, I), 30:50:20 (G, J), 40:40:20 (H, K). The scale bars are 300 nm in all the images.

Table 1. Characterizations of terpolymer and DOX-loaded micelles.

PEG:SA:CPP (mol%) ^{a)}	PEG:SA:CPP (mol%) ^{b)}	Mw ^{c)} ($\times 10^4$)	Morphology ^{d)}	Z-average(nm) ^{e)}	EE(%) ^{f)}	LC(%) ^{f)}
20:60:20	15.8:68.5:15.7	1.05	F	268 \pm 12.3	75.1 \pm 3.3	10.6 \pm 0.3
30:50:20	25.6:57.6:16.8	0.87	R	120 \pm 6.8	68.8 \pm 2.9	7.4 \pm 0.5
40:40:20	34.2:49.3:16.5	0.71	S	65 \pm 1.9	70.5 \pm 3.1	5.2 \pm 0.3

^{a)}Molal composition in feed; ^{b)}Molal composition determined by in ¹H NMR; ^{c)}Obtained by GPC; ^{d)}Visualized by AFM and TEM; ^{e)}Determined by DLS; ^{f)}Measured by UV-vis spectrophotometer. Feed weight ratio (drug/polymer = 1: 5).

capability of loading drug and longer circulation time *in vivo* than spherical nanoparticles.^[22]

2.3. Critical Micelle Concentration (CMC)

In order to determine the CMC of poly(PEG:CPP:SA) micelles, fluorescence measurements were carried out using pyrene as a fluorescent probe.^[49] When the concentration is increased as the micelles form, pyrene becomes encapsulated into the hydrophobic core of the micelle. Therefore, a red shift of characteristic peak in the emission spectra and an obvious increase in the intensity can be observed as shown in **Figure 2A**, which is the spectra of poly(PEG:CPP:SA) (30:50:20). The CMC of three different polymeric micelles can be obtained by plotting the I₃₃₉/I₃₃₃ band ratio of each curve in the excitation spectra versus logarithm of polymer concentration. In **Figure 2B**, below a certain

concentration, the I₃₃₉/I₃₃₃ band ratio did not change apparently, above the concentration, the ratio increases with increasing log C. From this plot, CMC is calculated by the intersection of two tangent of the curve. The CMC values of poly(PEG:CPP:SA) (20:60:20) was determined to be 0.00259 mg/mL. In **Figure 2C-D** the CMC values of 0.00301 mg/mL and 0.00381 mg/mL were also obtained from other two curves for poly(PEG:CPP:SA) with PEG/CPP/SA ratios of 30:50:20 and 40:40:20, respectively. The values decrease slightly with hydrophobic segment as the core increases, which is in agreement with previous reports on amphiphilic copolymers, in which it has been demonstrated that a larger or longer hydrophobic segment facilitates and stabilizes the conformation of micelles.^[50,51] The quite low CMC value indicates the amphiphilic molecule has a strong tendency toward formation of micelles and so the polymeric micelle possess good stability for the drug in the suspension and great resistance to being diluted even within the body.

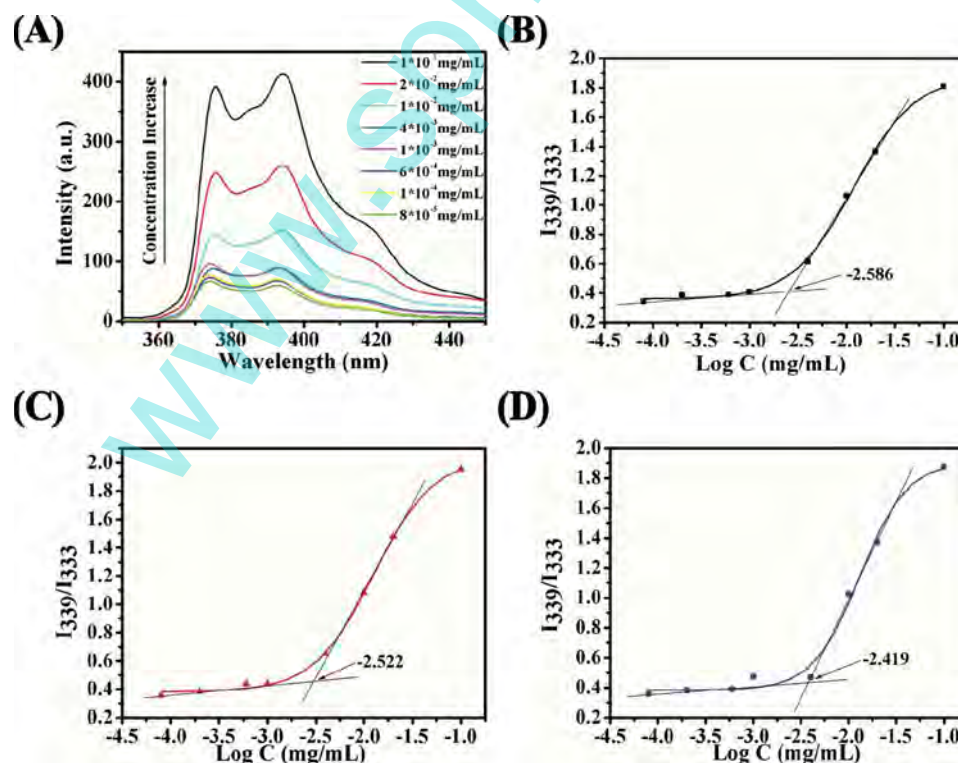


Figure 2. The fluorescence emission spectra of pyrene as a function of poly(PEG:SA:CPP) (30:50:20) concentration in water (A); Plot of change of intensity ratio (I₃₃₉/I₃₃₃) versus logarithm of poly(PEG:SA:CPP) concentrations with PEG/SA/ CPP ratios of 20:60:20 (B), 30:50:20 (C) and 40:40:20 (D).

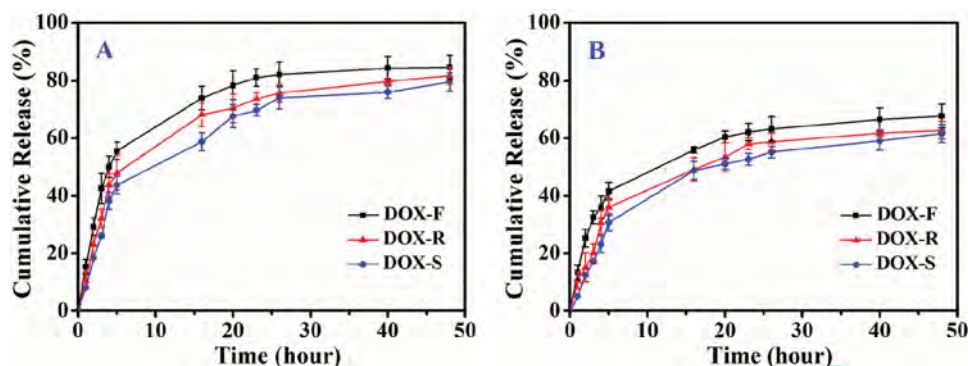


Figure 3. *In vitro* drug release profiles of DOX-loaded micelles with different morphologies in ABS at pH 5.0 (A) and PBS at pH 7.4 (B) at 37%, respectively. The error bars were calculated as standard deviation from triplicate samples.

2.4. Drug Loading, Encapsulation Efficiency and *In Vitro* DOX Release Study

We studied the effect of different feed ratios (drug/polymer = 1:20, 1:10 and 1:5) on the DOX loading content (LC) and encapsulation efficiency (EE). We found that LC and EE increased with the feed weight ratio of drug to polymer, when feed ratio was 1:5, they reached the highest value, especially for the filamentous micelles as exhibited in Table 1 (The results of 1:20 and 1:10 were not shown).

Subsequently the *in vitro* DOX-release study was performed. Figure 3 shows the DOX release behaviors in ABS at pH 5.0 and PBS at pH 7.4, respectively. From the two-stage-release profiles, we can observe an apparent initial burst in the original 5 h, followed by a sustained release over a prolonged period of time. The initial burst was mainly caused by certain amount of drug located within the hydrophilic shell or at the interface between the unimolecular micelles. Compared with the DOX release profile at pH 7.4, the release rate at pH 5.0 was much faster. This is mainly ascribed to the increased solubility of DOX at acidic pH upon protonation of the glycosidic amine.^[52] The accelerated DOX release in acidic pH condition is highly desirable for effective treatment of cancer. As well known, the pH value of cytoplasm inside normal cells is 7.4 while the pH value of the endocytic compartments in tumor cells are weakly acidic. Thus, the DOX-loaded micelles can realize promptly intracellular release of DOX in tumor cells, and normal cells and tissues can be avoided to be destroyed.

In particular, from Figure 3 we find that the micellar shape has an effect on the DOX release behavior. At the same pH condition, the DOX release from the filamentous micelles was the fastest, and the rate of spherical micelles was the lowest. The reason may be ascribed to two aspects. One is the difference in drug loading among the three types of micelles. The DOX loading in filamentous micelles is the highest, as shown in Table 1. The DOX release is influenced by the drug loading content or drug density in the micelles. The release from polymeric micelles is also a diffusion process depending on the drug payload.^[53] The other is that under the mechanical shaking (100 cycles/min), the non-spherical micelles have poorer ability to resist the shaking,

which caused partial fragmentation of micelles as previous reports.^[18,43]

2.5. *In Vitro* Cytotoxicity of Blank and DOX-Loaded Micelles

To appraise the biocompatibility of the polymeric blank micelles, A549, HepG2 and KB tumor cells were co-cultured with micelles at different concentrations ranging from 20 to 80 $\mu\text{g/mL}$, respectively. Figure 4 shows that the mean cell viability of three different tumor cells exceeds 90% against the blank micelles with filamentous, rod-like and spherical morphologies after co-incubation for 48 h. It demonstrated that all micelles were no significant cytotoxicity at tested concentrations, suggesting that these polymer micelles possess good biocompatibility.

Additionally, to examine the pharmacological activity of DOX-loaded micelles, IC_{50} were also evaluated through co-culture mixed with the A549, HepG2 and KB cells and drug-loaded micelles after 48 h. We can also find that the inhibition effect of micelles to tumor cell growth was also influenced by their shapes. Figure 4 exhibits that the cell viability was examined after 48 h of incubation with a series of doses of free DOX and DOX-loaded micelles with the three shapes using Alamar blue assay. It can be observed that the cytotoxicity of all DOX-loaded micelles is lower than that of free DOX at DOX concentrations ranging from 0.01 to 4.0 $\mu\text{g/mL}$. The IC_{50} values of the free DOX against A549 ($\text{IC}_{50} = 0.31 \mu\text{g/mL}$), HepG2 ($\text{IC}_{50} = 0.59 \mu\text{g/mL}$) and KB ($\text{IC}_{50} = 1.26 \mu\text{g/mL}$) cells are different but the values are the lowest compared with DOX-loaded micelles. Moreover, the IC_{50} values of the free DOX would seriously damage the normal cells. Here, different tumor cell lines have the different resistance against the free DOX, and KB cells have a much higher IC_{50} value than other cancer cell lines because of their severe multi-drug resistance (MDR) effect.^[54] Interestingly, the DOX-loaded micelles with different morphologies have different inhibition effects against the three tumor cell lines. For A549 cells, spherical DOX-loaded micelles ($\text{IC}_{50} = 0.61 \mu\text{g/mL}$) have the higher inhibition ratio than filamentous ($\text{IC}_{50} = 1.12 \mu\text{g/mL}$) and rod-like ($\text{IC}_{50} = 1.04 \mu\text{g/mL}$) micelles. For HepG2 cells, there is little difference among the three DOX-loaded micelles for the IC_{50} value. In comparison, for KB cells

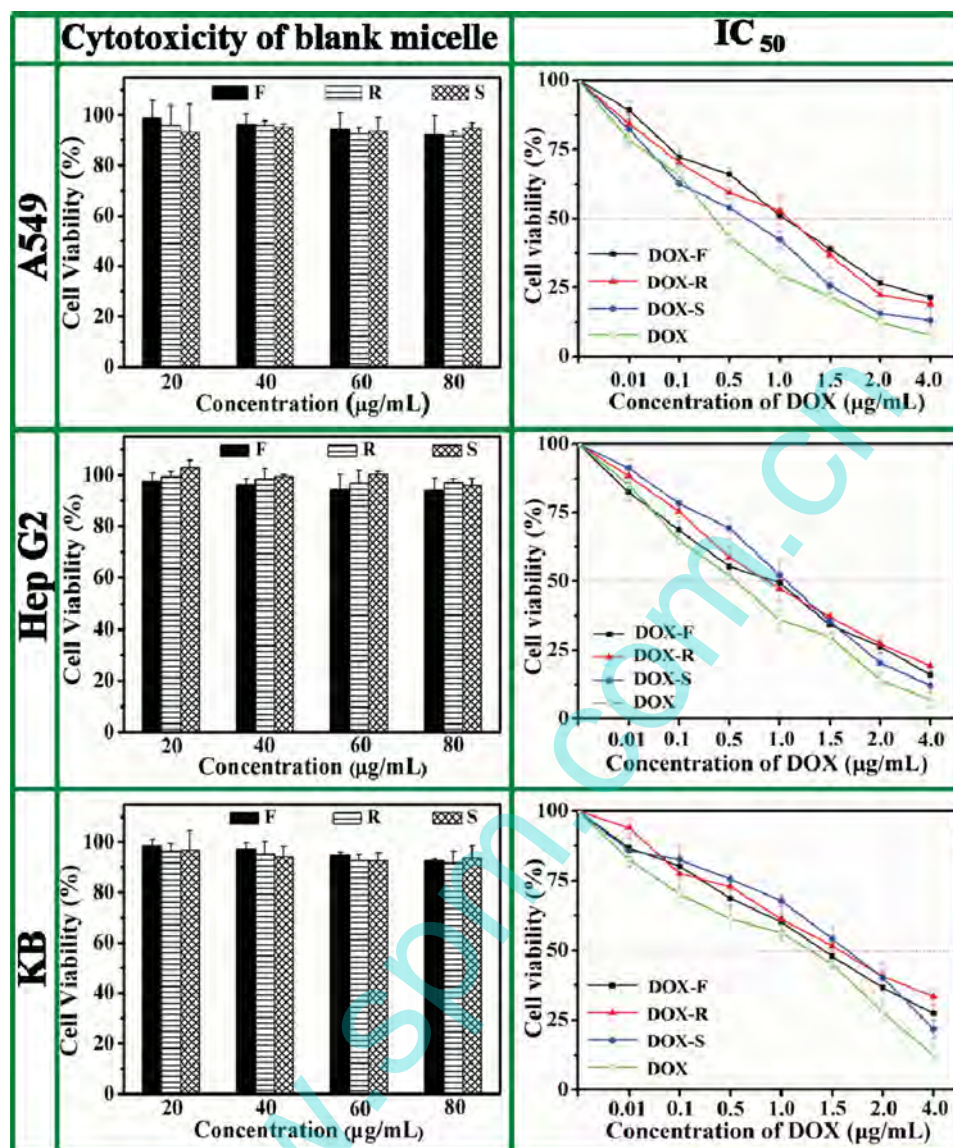


Figure 4. *In vitro* cell viability of A549, HepG2 and KB cells. Tumor cells were exposed to various concentrations of free DOX, blank and drug-loaded micelles with different shapes for 48 h, respectively. The standard deviation for each data point averaged over 3 samples.

filamentous DOX-loaded micelles ($IC_{50} = 1.41 \mu\text{g/mL}$) have the lowest IC_{50} value.

2.6. The Effect of Micellar Shape on Cellular Uptake

To investigate the effect of the carrier shapes on cellular uptake in fibroblast normal cells, A549, HepG2 and KB tumor cells, fluorescence microscopy and CLSM were employed to visualize a short-term micelle endocytosis. **Figure 5A** exhibits fluorescence microscopy images of drug-loaded micelles of different morphologies endocytosed in these cells. Five incubation times (0.25, 0.5, 1, 3 and 6 h) were chosen for the test. For fibroblast normal cells, very weak red fluorescence can be observed within original 1 h for all the groups exposed with the three types of

DOX-loaded micelles. When the time increased to 6 h, red fluorescence could be detected, especially for the DOX-S. It can be elucidated that spherical micelles were readily to be taken up compared with the DOX-R and DOX-F. For A549 tumor cells, a remarkable time-dependent cellular uptake behavior was also observed. At 3 h, the significant red fluorescence was observed for the cells cultured with DOX-S, but red fluorescent in other groups were weaker. During the short-term test, similar time-dependent cellular uptake behaviors were also observed for HepG2 and KB cell lines, and the fluorescence intensities in DOX-S groups were still the most obvious. Therefore, it can be concluded that spherical micelles were more easily to be taken up by all the cells tested.

To further analyze the cellular uptake efficiency of DOX-loaded micelles of different morphologies, a quantitative

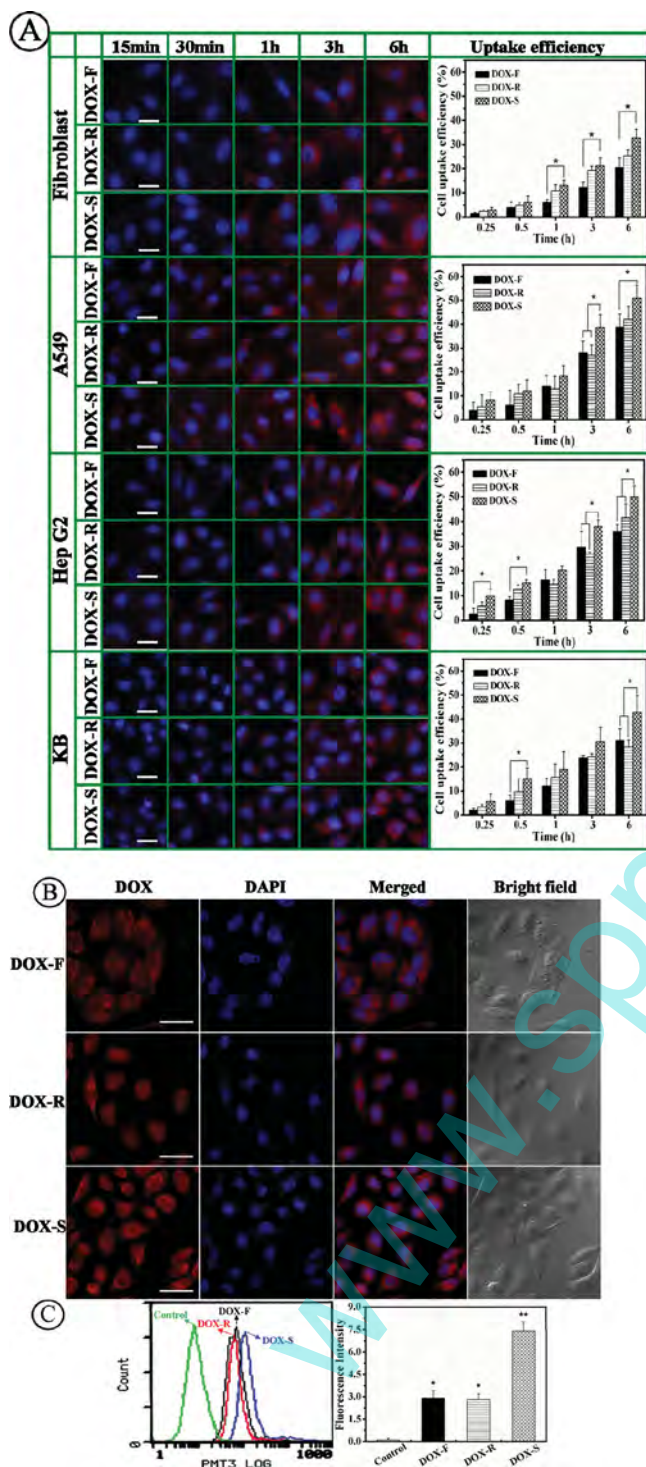


Figure 5. (A) Fluorescence microscopy images and cell uptake efficiency of fibroblast, A549, HepG2 and KB cells incubated with filamentous, rod-like and spherical DOX (Red)-loaded micelles for 0.25, 0.5, 1, 3 and 6 h, respectively, the scale bars are 30 μm in all the images and cell nucleus stained with DAPI (Blue). Quantitatively analyzed using Image-Pro Plus 6.0 software. * $P < 0.05$ versus filamentous and rod-like DOX-loaded micelles. (B) Confocal laser scanning microscopy (CLSM) images, (C) flow cytometry histograms and mean fluorescence intensity show the A549 cells treated with DOX-loaded micelles of different morphologies with 5 $\mu\text{g}/\text{mL}$ DOX (3 h incubation). * $P < 0.05$ versus control.

examine was also carried out on the fibroblast normal cells and the tumor cell lines using Image-Pro Plus 6.0 software. As shown in Figure 5A, the same intervals as the test above were also chosen. These results also confirmed that cellular uptake of drug-loaded micelles in tumor cells increased with incubation time. In addition, the cellular uptake efficiency can also be influenced by the morphology of the micelle for the fibroblast normal cells and tumor cells. These results demonstrated that spherical micelles are prone to be taken up by the cells due to the micellar size and morphology.^[31]

CLSM images were shown in Figure 5B to further characterize the different cellular uptake efficiencies of DOX-loaded micelles of different morphologies for A549 cell lines at 3 h. The higher intracellular DOX fluorescence intensity was also observed in the cells incubated with DOX-S. It was demonstrated that there were more DOX-S accumulated into the cells than the other two groups.

Flow cytometric analyzer was employed to further quantify the effect of micellar shape on the cellular uptake efficiency. Figure 5C exhibits the distribution of fluorescence intensity of the A549 cells exposed with the DOX-F, DOX-R, DOX-S and untreated for 3 h. We can find that the mean fluorescence intensities in all micelle groups are much higher than the control group. Among the three types of micelles, the intensity of the DOX-S is slightly higher than the other two micelles, also indicating that the DOX-S can be taken up more easily by tumor cells, which is very consistent with discussed above.

For the uptake mechanism of the particles, there have been two main internalization pathways: phagocytosis or endocytic pathways. When the particle dimension exceed 1 μm , phagocytosis or macropinocytosis play the major role therefore need to be form large endocytic vesicles from the cell membrane; if the diameter of nanoparticles is less than 100 nm or smaller, caveolae-mediated endocytosis pathway, which form cell membrane invagination coated with caveolin, will occurs.^[31,55] Herein, three different shaped micelles were applied to explore the effect of morphology on cellular uptake. It is noteworthy that the smaller micelle, the higher the uptake efficiency. There is an optimal size for enveloping efficiently, which is 54-60 nm in diameter, which has been portended theoretically. It has been reported that the endocytic vesicles formed in the early stage are smaller than 100 nm in diameter.^[56] Here, the spherical micelles (average length = 65 nm) are smallest in diameter, so they are readily to be taken up in a short time through caveolae-mediated endocytosis pathway. Whereas most rod-like micelles (Length = 280 nm) have to be curved or fragmented to be endocytosised, which demand added energy. In this case, the longer the “enveloping time” is, the slower the cellular uptake is. Furthermore, the filamentous micelles are the longest in length (Length = 1200 nm), they are supposed to be fractionized or bent in order to be enfolded in large endocytic vesicles, which require more energy, through phagocytosis or macropinocytosis. The energy dependency of the uptake process requires time. Therefore the cellular uptake is dependent on micellar size and shape.

2.7. The Impact of Micellar Shape on *In Vivo* Antitumor Effect

The impact of the carrier shape on *in vivo* antitumor effect was assessed using 4T1 bearing mice as an animal model.

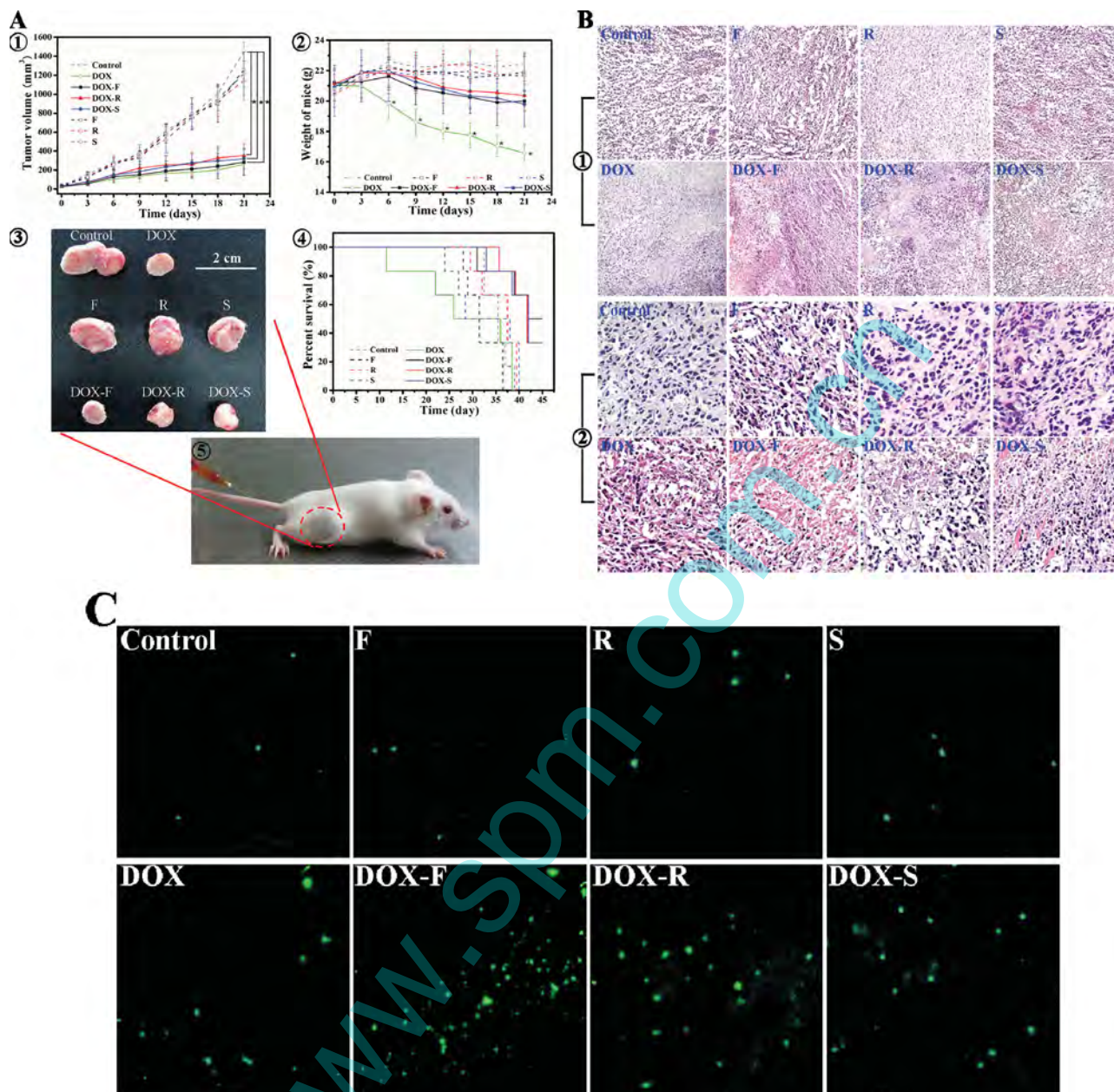


Figure 6. (A) *In vivo* antitumor activity and systemic toxicity of free DOX and DOX-loaded micelles injected into BALB/c mice at a dose of 5 mg/kg: (1) Tumor volumes of different treatment groups. Results are means \pm SD ($n = 6$), (2) Body weight changes of 4T1 tumor bearing mice ($n = 6$), (3) Excised 4T1 solid tumors from different treatment groups (Scale bars, 2 cm), (4) Survival curves of mice with 4T1 breast tumors, (5) Digital photos of BALB/c mice with 4T1 breast tumors established by subcutaneous injection. * $P < 0.05$ versus control. (B) H&E stained tumor tissue slices from mice at the 21st day in various controls and experimental groups. Original magnification: $\times 100$ (1) and $\times 400$ (2). (C) Effect of micellar shape on the apoptosis of tumors at the 21st day. Tumor apoptotic cells were discovered by TUNEL assay, TUNEL-positive signals were denoted green. Original magnification: $\times 400$.

Figure 6A1-3 show that all the DOX-loaded micelles were effective in inhibiting tumor growth compared with treatments with 0.9% saline solution and blank micelles. From Figure 6A1, we can also find that the growth rate of the tumor in free DOX and DOX-loaded micelle groups was much lower than these groups without DOX. The final tumor volumes in these groups treated with DOX-S, DOX-R and DOX-F was around 300 ± 10 , 280 ± 10 and 230 ± 10 mm³, respectively, which was significantly

smaller than these groups without DOX ($P < 0.05$). At the 21st day the tumor inhibition ratios calculated from tumor volume were 77.2%, 79.5% and 85.6% for DOX-S, DOX-R and DOX-F, respectively. These results indicated that DOX-F had the best antitumor effect. Additionally, free DOX also showed significant tumor inhibition. From Figure 6A2, we can find the weight of the mice in free DOX group decreased obviously with feeding period increased compared with other groups, indicating that

free DOX indeed have serious systemic toxicity to body. On the contrary, when free DOX was encapsulated in these polymer micelles with spherical, filamentous and rod-like shapes, its negative side effect can be restrained greatly. Figure 6A4 represents the survival of 4T1 tumors-bearing mice in response to different treatments. It can be illustrated that the three kinds of DOX-loaded micelles were more effective in prolonging the mice survival than other groups, furthermore mice treated with DOX-F had a longer survival time compared with DOX-R and DOX-S groups, suggesting it possessed better antitumor effect and higher safety to body.

2.8. Histological Examination

To reveal the possible mechanism involved, immunostainings of tumor sections for the analysis of tumor cell proliferation *in vivo* were performed. The apoptosis induced within tumors was evaluated after intravenous administration of 0.9% saline solution (Control) and the spherical (S), rod-like (R) and filamentous (F) micelles with and without DOX as shown in Figure 6B. From Figure 6B1, we can find that there were a lot of apoptotic cells or necrotic areas throughout the tumor excised from 4T1 bearing mice treated with free DOX and DOX-loaded micelles, on the other hand, the number of apoptotic cells within the tumor was markedly smaller in the control and blank micelle groups. In order to observe the H&E-stained sections of tumors more clearly, the original magnification of 400 times was performed (Figure 6B2). Indeed, tumor remnants with significant necrosis and many apoptotic cells were typically found in DOX-F, DOX-R and DOX-S groups, especially for DOX-F group the feature was the most remarkable, whereas the cells were almost not influenced in the control and blank micelle groups. The result also demonstrated that the micellar formulation had better capacity to deliver DOX in cancer treatment, especially for the filamentous micelles with a high aspect ratio. TUNEL staining was performed to further assess whether DOX-loaded micelles induced apoptosis in 4T1 solid tumors. As shown in Figure 6C, we can also observe that DOX-F induced more tumor cells apoptosis compared to the other groups, whereas the therapeutic effect of the same dosage of free DOX was indistinctive. To our knowledge, to date few literatures has reported that DOX-loaded filamentous micelles hold such antitumor capacity to artificial solid tumor in mice. The reason that DOX-F having the best therapeutic effect *in vivo* could be attributed to the long-circulating feature of the shape and diameter of nanoscale (<100 nm), which can reduce the phagocytosis by cells of the mononuclear phagocyte system in blood flow and allow them to penetrate exceedingly small interspace.^[55]

3. Conclusions

In summary, filamentous, rod-like and spherical DOX-loaded micelles were prepared from poly(ether-anhydrides) terpolymers. The influence of the micellar shape on its functions as a nanocarrier including drug release behavior and cellular internalization in the normal and tumor cells *in vitro* and their therapeutic effect to solid tumor *in vivo*, was investigated.

The filamentous micelles possessed the highest DOX loading capacity and encapsulation efficiency among the different types of micelles. The *in vitro* release behaviors show that the drug release performance of the micelles was dependent on carrier shape. The results from *in vitro* cytotoxicity analysis and cellular uptake with HepG2, KB, and A549 cells demonstrate that all the micelles have excellent biocompatibility and the DOX-loaded micelles are effective at inhibiting the growth of tumor cells. These quantitative and qualitative results of cellular uptake demonstrate that the spherical micelles were most easily taken up by all types of cells. The results of *in vivo* antitumor activity demonstrate that the filamentous DOX-loaded micelles possess the highest safety to body and the best therapeutic effect towards artificial solid tumor. Therefore, the filamentous micelle can be developed to a high-potential formulation to deliver antitumor drugs in the treatment of cancers.

4. Experimental Section

Preparation of Blank and DOX-loaded Micelles: The amphiphilic poly(PEG:SA:CPP) terpolymers composed of SA, CPP and PEG were synthesized via melt-condensation polymerization per our previous report.^[57] The blank micelles were fabricated by using a solvent evaporation method.^[58] In brief, preweighed poly(PEG:SA:CPP) terpolymers were dissolved in 5 mL tetrahydrofuran (THF), and the solution of the copolymer was added dropwise using a disposable syringe (21 gauge) under high speed stirring into 10 mL deionized water. The mixed solution was then stirred moderately for 4 h at room temperature to evaporate the THF completely and fabricate polymeric micelles. By altering the ratio of PEG and SA in the terpolymers, micelles with spherical (S), rod-like (R) or filamentous (F) shapes could be obtained. The procedure of fabricating the DOX-loaded micelles was almost similar with mentioned above. The slight difference is that after the THF was evaporated completely, the drug-loaded micelles were transferred into dialysis bag (MWCO 1000) with distilled water to remove the unloaded DOX.

Characterization: To confirm the chemical structure of the terpolymer, Fourier transform Infrared spectra (FT-IR) were taken using a Nicolet 5700 spectrometer. KBr tablets were prepared by grinding the polymer sample with KBr and compressing the whole into a semitransparent tablet. ¹H-NMR spectra were obtained on a Bruker AM 300 apparatus. CDCl₃ and Tetra-methylsilane (TMS) were used as the solvent and internal reference respectively. Chemical shifts were expressed as parts per million, ppm (δ). Gel permeation chromatography (GPC) was performed with a Water 2695 separation module equipped with a Styragel HT4DMF column calibrated with polystyrene narrow standards operated at 40% and series 2414 refractive index detector. To examine the average size and size distribution of micelles in distilled water, dynamic light scattering (DLS) (ZETA-SIZER, MALVERN Nano-ZS90, Malvern Ltd., U.K.) was employed. The experimental temperature was 25%. All the experiments were carried out in triplicate. Atomic force microscopy (AFM) (CSPM5000, Being, China) was employed to discern the morphologies of the micelles. Tapping-mode AFM was utilized to scan the sample after the sample-loaded silicon wafer was dried for 5 h at atmospheric pressure at room temperature. The morphologies and size of the micelles were also observed at 150 kV with a Transmission Electron Microscope (TEM) (Hitachi H-700H, Japan). Micelle samples for TEM were prepared by dipping a droplet of the micellar solution on a Formvar-coated copper grid and dried in air before being stained with phosphotungstic acid aqueous solution (2% w/w). Critical micelle concentration (CMC) of micelles with different morphologies was determined by pyrene as a fluorescent probe. Fluorescence spectra were recorded on a Fluoromax spectrometer (F-7000, Hitach, Japan) at room temperature. The emission wavelength and excitation bandwidth were

set at 390 and 5 nm, respectively. The fluorescence intensity ratio of I339/I333 was analyzed as a function of micelle concentration.

Analysis of Drug Loading and Encapsulation Efficiency: Drug loading content (LC) and encapsulation efficiency (EE) were measured with UV-vis spectrophotometer (UV-2550, Shimadzu, Japan). The DOX-loaded micelles of different morphologies with different drug loadings were prepared and lyophilized. Preweighed the lyophilized micelle powder was dissolved in 3 mL DMSO, and its absorption at 488 nm was determined by UV. LC and EE were calculated by Equation 1 and 2, respectively.

$$LC\% = \frac{\text{Weight of the drug in micelles}}{\text{Weight of micelles}} \times 100\% \quad (1)$$

$$EE\% = \frac{\text{Weight of the drug in micelles}}{\text{Weight of the drug in feed}} \times 100\% \quad (2)$$

In vitro DOX Release from Micelles with Different Shapes: In vitro drug release from polymer micelles was studied by using cellulose ester dialysis membrane bags with a cut off molecular weight of 1000 g/mol at 37% in phosphate buffered solution (PBS) at pH 7.4 and acetate buffered solution (ABS) at pH 5.0, respectively. The dialysis bags were immersed into corresponding buffer in a prepared tube with a shaking at 100 cycles/min under a predetermined sink condition. 1 mL of release media was taken out and replenished with an equal volume of fresh media at predetermined time points. Concentration of DOX released was also determined by UV-visible spectrophotometry at absorbance of 488 nm. The release experiments were conducted in triplicate. The results presented are the average data.

In vitro Cytotoxicity Analysis: The cytotoxicity of the blank micelles of different morphologies and tumor cell inhibitions of DOX-loaded micelles were evaluated by Alamar blue assays. Human hepatoblastoma cell line (HepG2), lung epithelial cancer cell lines (A549), human nasopharyngeal epidermoid carcinoma cells (KB) were seeded at a density of 1.0×10^4 cells/well onto 48-well plates in RPMI 1640 supplemented with 10% fetal bovine serum (FBS) and maintained at 37% in a humidified incubator with 5% CO₂ and 95% air. After 24 h, the medium was replaced with 1.0 mL of fresh medium and subsequently combined with the respective micellar and DOX-loaded micellar solution of different morphologies. The concentration of blank micellar solutions ranged from 20 to 80 µg/mL and DOX-loaded micelles with DOX content varied from 0.01 to 4.0 µg/mL were added to incubate. After 48 h, medium was carefully removed and 300 µL Alamar blue solution (10% Alamar blue, 80% media 199 (Gibcos) and 10% FBS; V/V) was added into each well and incubated for 4 h further at 37%, 5% CO₂. A sample of 200 µL of reduced Alamar blue solution was pipetted into costar opaque black bottom 96-well plate (Sigma) and the plates were read in an automated microplate spectrophotometer (ELX800 Biotek, USA) at 570 nm as reference. Results are the mean ± standard deviation of three experiments performed in triplicate.

Evaluation of Cellular Uptake: For qualitative cellular uptake analysis, fibroblast, HepG2, A549 and KB cells were seeded into 6-well plates with a density of 1.0×10^5 cells/well with 2 mL RPMI 1640 medium. The cells were kept in the incubator at 37% in humidified atmosphere containing 5% CO₂. After incubation for 24 h, free DOX solution and the micellar solutions with spherical (S), rod-like (R) and filamentous (F) shapes with a same dosage of 5 µg/mL DOX were added into each 6-well plate, respectively. After incubation for predetermined times, the medium was removed and the wells were washed with PBS. The cells were then fixed with 2.5% glutaraldehyde for 30 min and the cell nuclei were stained with 4',6-diamidino-2-phenylindole (DAPI, blue) for three min. The fluorescence images of DOX-S, DOX-R and DOX-F in the desired cells were acquired by an inverted fluorescence microscope (Olympus, CKX41) with a charge-coupled device camera (Imaging, Micropublisher 5.0 RTV) and a mercury lamp (Olympus, U-RFLT50) and quantitatively analyzed using Image-Pro Plus 6.0 software.^[59] The cellular uptake efficiency was calculated as the percent of the fluorescence intensity of the testing cells over that of the positive control group. In order to investigate the

influence of the micellar shape on the uptake quantitatively, the cells were also analyzed by flow cytometry (Epics Elite EST, USA).

Animals and Tumor Inoculation: All animal studies were approved by the Institutional Animal Care and Use Committee of Sichuan University and were in compliance with all regulatory guidelines. Murine breast cancer cells 4T1 (2×10^5 cells, 100 µL per mouse) were inoculated into female Balb/c mice (6 ~ 7 weeks, 20 ± 2 g) subcutaneously in the right back area. Tumor volume was calculated with vernier calipers by measuring two dimensions and using the equation: Volume (mm³) = $a \times b^2 \times 0.5$, where a and b are the longest and the shortest diameter, respectively.

In vivo Antitumor Activity: Murine breast cancer cells 4T1 (2×10^5 cells) were implanted in the right back area of the mice subcutaneously. When the tumor reached a mean size of approximately 50 mm³ in volume (named as Day 0), treatments were carried out. At that time, 48 mice were randomly assigned to a control group and seven experimental groups of 6 mice each. Animals were treated seven times at an interval of 3 days for a total of 21 days with each of the samples listed below: 0.9% saline solution (control); free DOX; spherical (S), rod-like (R) and filamentous (F) blank micelles as well as their relevant DOX-loaded micelles at an equivalent DOX dose of 5 mg/kg. Each formulation was administered to the animals by tail vein injection. The mice were sacrificed on day 21, the tumor tissues were collected and some of them were fixed in neutral 10% formalin solution subsequently and part of them were frozen in liquid nitrogen for frozen section. The tumor inhibition activity was assessed with tumor volume measured with a vernier caliper. The body weight was measured simultaneously. For the survival study, 48 mice were randomized into eight groups (6 mice per group), the dose and frequency injected were the same as above and the survival data was recorded daily throughout the test time.

Histological Examination: All the tissues fixed were operated routinely: paraffin-embedded, sectioned and stained with hematoxylin and eosin (H&E). The histological slices obtained were observed by optical microscopy. Terminal deoxynucleotidyl transferase dUTP nick end labeling (TUNEL) staining was used to evaluate the apoptosis of tumor cells at the 21st day.

Statistical Analysis: For all the experiments, data are presented as mean ± standard deviation. The statistical significance of the results was analyzed using SPSS (version 16). Differences between experimental groups were compared by Student t-test. The results were considered to have a statistically significant difference if $p < 0.05$.

Acknowledgements:

This work was partially supported by National Natural Science Foundation of China (No.30970723 and No.51173150) and National Basic Research Program of China (973 Program, 2012CB933602).

Received: December 9, 2012

Published online:

- [1] R. C. Mundargi, V. R. Babu, V. Rangaswamy, P. Patel, T. M. Aminabhavi, *J. Controlled Release* **2008**, 125, 193.
- [2] M. Dunne, O. I. Corrigan, Z. Ramtoola, *Biomaterials* **2000**, 21, 1659.
- [3] J. Panyam, V. Labhasetwar, *Adv. Drug Deliver. Rev.* **2003**, 55, 329.
- [4] J. Rejman, V. Oberle, I. S. Zuhorn, D. Hoekstra, *Biochem. J.* **2004**, 377, 159.
- [5] H. Gao, W. Shi, L. B. Freund, *Proc. Natl. Acad. Sci. USA* **2005**, 102, 9469.
- [6] W. Jiang, B. Y. S. Kim, J. T. Rutka, W. C. W. Chan, *Nat. Nanotechnol.* **2008**, 3, 145.
- [7] W. J. Wang, S. B. Zhou, L. Y. Guo, W. Zhi, X. H. Li, J. Weng, *Int. J. Nanomed.* **2010**, 5, 557.
- [8] R. Gref, Y. Minamitake, M. T. Peracchia, V. Trubetskoy, V. Torchilin, R. Langer, *Science* **1994**, 263, 1600.

- [9] S. Stolnik, L. Illum, S. S. Davis, *Adv. Drug Deliver. Rev.* **1995**, *16*, 195.
- [10] G. Storm, S. O. Belliot, T. Daemen, D. D. Lasic, *Adv. Drug Deliver. Rev.* **1995**, *17*, 31.
- [11] H. F. Liang, C. T. Chen, S. C. Chen, A. R. Kulkarni, Y. L. Chiu, M. C. Chen, H. W. Sung, *Biomaterials* **2006**, *27*, 2051.
- [12] J. A. Champion, Y. K. Katare, S. Mitragotri, *J. Controlled Release* **2007**, *121*, 3.
- [13] A. Verma, F. Stellacci, *Small* **2010**, *6*, 12.
- [14] J. A. Champion, S. Mitragotri, *Proc. Natl. Acad. Sci. USA* **2006**, *103*, 4930.
- [15] F. Ahmed, D. E. Discher, *J. Controlled Release* **2004**, *96*, 37.
- [16] Y. Geng, D. E. Discher, *Polymer* **2006**, *47*, 2519.
- [17] F. Ahmed, R. I. Pakunlu, G. Srinivas, A. Brannan, F. Bates, M. L. Klein, T. Minko, D. E. Discher, *Mol. Pharmaceut.* **2006**, *3*, 340.
- [18] S. Cai, K. Vijayan, D. Cheng, E. M. Lima, D. E. Discher, *Pharm. Res.* **2007**, *24*, 2099.
- [19] S. E. A. Gratton, P. A. Ropp, P. D. Pohlhaus, J. C. Luft, V. J. Madden, M. E. Napier, J. M. DeSimone, *Proc. Natl. Acad. Sci. USA* **2008**, *105*, 11613.
- [20] G. Sharma, D. T. Valenta, Y. Altman, S. Harvey, H. Xie, S. Mitragotri, J. W. Smith, *J. Controlled Release* **2010**, *147*, 408.
- [21] X. Huang, X. Teng, D. Chen, F. Tang, J. He, *Biomaterials* **2010**, *31*, 438.
- [22] Y. Geng, P. Dalhaimer, S. Cai, R. Tsai, M. Tewari, T. Minko, D. E. Discher, *Nat. Nanotechnol.* **2007**, *2*, 249.
- [23] S. Muro, C. Garnacho, J. A. Champion, J. Leferovich, C. Gajewski, E. H. Schuchman, S. Mitragotri, V. R. Muzykantov, *Mol. Ther.* **2008**, *16*, 1450.
- [24] N. Doshi, B. Prabhakarandian, A. Rea-Ramsey, K. Pant, S. Sundaram, S. Mitragotri, *J. Controlled Release* **2010**, *146*, 196.
- [25] H. Meng, S. Yang, Z. Li, T. Xia, J. Chen, Z. Ji, H. Zhang, X. Wang, S. Lin, C. Huang, *ACS. Nano* **2011**, *5*, 4434.
- [26] S. Y. Lin, W. H. Hsu, J. M. Lo, H. C. Tsai, G. H. Hsiue, *J. Controlled Release* **2011**, *154*, 84.
- [27] S. Mitragotri, J. Lahann, *Nat. Mater.* **2009**, *8*, 15.
- [28] R. A. Petros, J. M. DeSimone, *Nat. Rev. Drug Discov.* **2010**, *9*, 615.
- [29] M. Ferrari, *Nat. Rev. Cancer* **2005**, *5*, 161.
- [30] G. von Maltzahn, J. H. Park, K. Y. Lin, N. Singh, C. Schw Ppe, R. Mesters, W. E. Berdel, E. Ruoslahti, M. J. Sailor, S. N. Bhatia, *Nat. Mater.* **2011**, *10*, 545.
- [31] H. Hillaireau, P. Couvreur, *Cell. Mol. Life Sci.* **2009**, *66*, 2873.
- [32] E. M. Pridgen, R. Langer, O. C. Farokhzad, *Nanomedicine* **2007**, *2*, 669.
- [33] L. Tribler, L. T. Jensen, K. J. Rgensen, N. Br nner, M. H. Gelb, H. J. Nielsen, S. S. Jensen, *Anticancer Res.* **2007**, *27*, 3179.
- [34] Y. Wang, T. Yang, X. Wang, W. Dai, J. Wang, X. Zhang, Z. Li, Q. Zhang, *J. Controlled Release* **2010**, *149*, 299.
- [35] T. H. Kim, C. W. Mount, W. R. Gombotz, S. H. Pun, *Biomaterials* **2010**, *31*, 7386.
- [36] F. Ahmed, R. I. Pakunlu, A. Brannan, F. Bates, T. Minko, D. E. Discher, *J. Controlled Release* **2006**, *116*, 150.
- [37] X. Yang, J. J. Grailer, I. J. Rowland, A. Javadi, S. A. Hurley, D. A. Steeber, S. Gong, *Biomaterials* **2010**, *31*, 9065.
- [38] T. M. Allen, P. R. Cullis, *Science* **2004**, *303*, 1818.
- [39] X. Hu, S. Liu, X. Chen, G. Mo, Z. Xie, X. Jing, *Biomacromolecules* **2008**, *9*, 553.
- [40] A. Basarkar, J. Singh, *Pharm. Res.* **2009**, *26*, 72.
- [41] S. Jain, F. S. Bates, *Science* **2003**, *300*, 460.
- [42] F. Ahmed, D. E. Discher, *J. Controlled Release* **2004**, *96*, 37.
- [43] A. H. Lee, K. T. Oh, H. J. Baik, B. R. Lee, Y. T. Oh, D. H. Lee, E. S. Lee, *Bull. Korean Chem. Soc.* **2010**, *31*, 2265.
- [44] D. A. Christian, S. Cai, O. B. Garbuzenko, T. Harada, A. L. Zajac, T. Minko, D. E. Discher, *Mol. Pharmaceut.* **2009**, *6*, 1343.
- [45] K. Knop, R. Hoogenboom, D. Fischer, U. S. Schubert, *Angew. Chem. Int. Ed.* **2010**, *49*, 6288.
- [46] S. M. Moghimi, A. C. Hunter, J. C. Murray, *Pharmacol. Rev.* **2001**, *53*, 283.
- [47] J. Fiegel, J. Fu, J. Hanes, *J. Controlled Release* **2004**, *96*, 411.
- [48] A. S. Mikhail, C. Allen, *Biomacromolecules* **2010**, *11*, 1273.
- [49] C. L. Zhao, M. A. Winnik, G. Riess, M. D. Croucher, *Langmuir* **1990**, *6*, 514.
- [50] F. Zeng, H. Lee, M. Chidiac, C. Allen, *Biomacromolecules* **2005**, *6*, 2140.
- [51] C. L. Peng, M. J. Shieh, M. H. Tsai, C. C. Chang, P. S. Lai, *Biomaterials* **2008**, *29*, 3599.
- [52] M. Prabaharan, J. J. Grailer, S. Pilla, D. A. Steeber, S. Gong, *Biomaterials* **2009**, *30*, 3009.
- [53] Z. Zhu, Y. Li, X. Li, R. Li, Z. Jia, B. Liu, W. Guo, W. Wu, X. Jiang, *J. Controlled Release* **2010**, *142*, 438.
- [54] H. S. Yoo, T. G. Park, *J. Controlled Release* **2004**, *96*, 273.
- [55] R. A. Petros, J. M. DeSimone, *Nat. Rev. Drug Discov.* **2010**, *9*, 615.
- [56] F. Osaki, T. Kanamori, S. Sando, T. Sera, Y. Aoyama, *J. Am. Chem. Soc.* **2004**, *126*, 6520.
- [57] A. J. Zhao, Q. Zhou, T. Chen, J. Weng, S. B. Zhou, *J. Appl. Polym. Sci.* **2010**, *118*, 3576.
- [58] A. J. Zhao, S. B. Zhou, Q. Zhou, T. Chen, *Pharm. Res.* **2010**, *27*, 1627.
- [59] J. Wang, W. Liu, Q. Tu, J. Wang, N. Song, Y. Zhang, N. Nie, J. Wang, *Biomacromolecules* **2011**, *12*, 228.